Electronic Supporting Information

Single-Ion Chelation Strategy Synthesis of Monodisperse Pd Nanoparticles Anchored MOF-808 for Highly Efficient Hydrogenation and Cascade Reactions

Ke Zhao [1,2], Le-Xi Zhang [1]*, Heng Xu [1], Yi-Fei Liu [1], Bo Tang [1], Li-Jian Bie [1]*

[1] School of Materials Science and Engineering, Tianjin Key Lab for Photoelectric Materials and Devices, Key Laboratory of Display Materials and Photoelectric Devices (Ministry of Education), National Demonstration Center for Experimental Function Materials Education, Tianjin University of Technology, Tianjin 300384, China.

[2] MOE Key Laboratory of Cluster Science, Beijing Key Laboratory of Photoelectronic/Electrophotonic Conversion Materials, School of Chemistry and Chemical Engineering, Beijing Institute of Technology, Beijing 102488, China.

* Corresponding authors:

Le-Xi Zhang, Tel./Fax: +86 022 60214028. E–mail: lxzhang@tjut.edu.cn

Li-Jian Bie, Tel./Fas: +86 022 60215505.

E-mail: ljbie@tjut.edu.cn; ljbie@pku.org.cn

Contents

2

Section S1. Materials characterization.

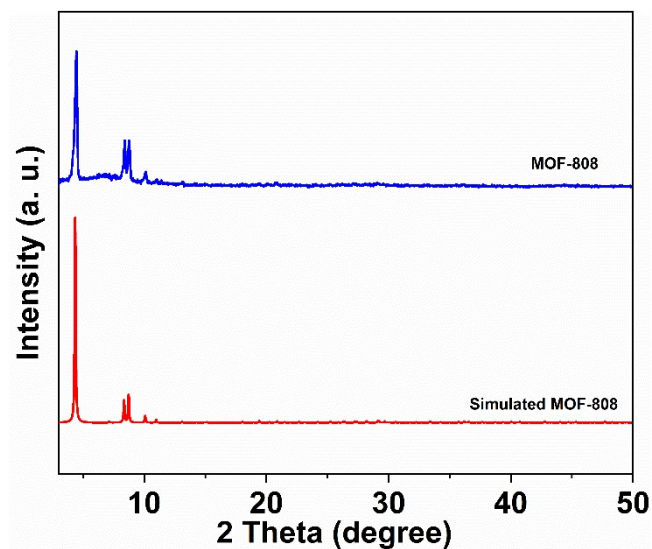**Section S1.1** Powder X-ray diffraction (PXRD).

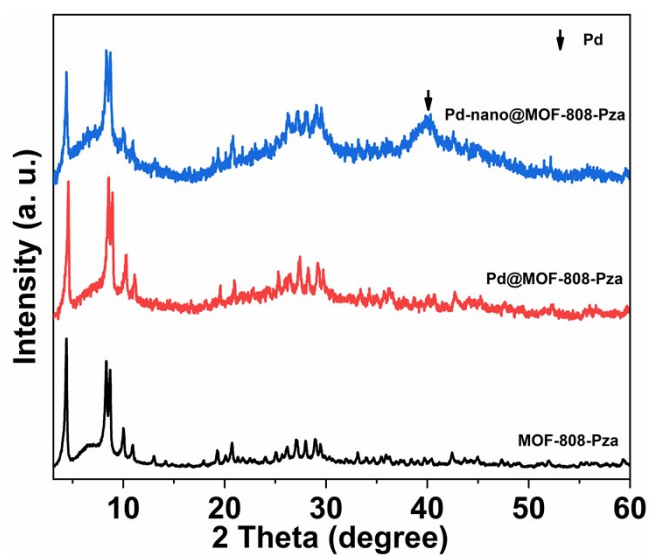**Figure S1.** PXRD patterns of as-prepared MOF-808 and simulated patterns of MOF-808.

Figure S2. PXRD patterns of MOF-808-Pza, Pd@MOF-808-Pza, and Pd-nano@MOF-808-Pza, respectively.
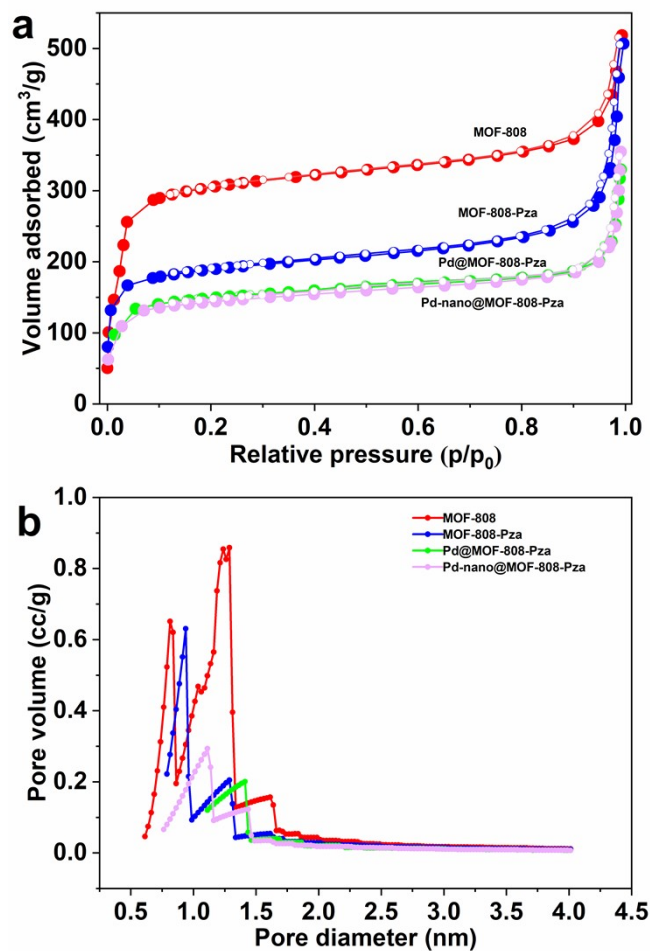
Section S1.2 Nitrogen adsorption measurements.

Figure S3. Nitrogen adsorption isotherms of MOF-808, MOF-808-Pza, Pd@MOF-808-Pza, and Pd-nano@MOF-808-Pza (a), as well as their calculated pore size distribution (b).

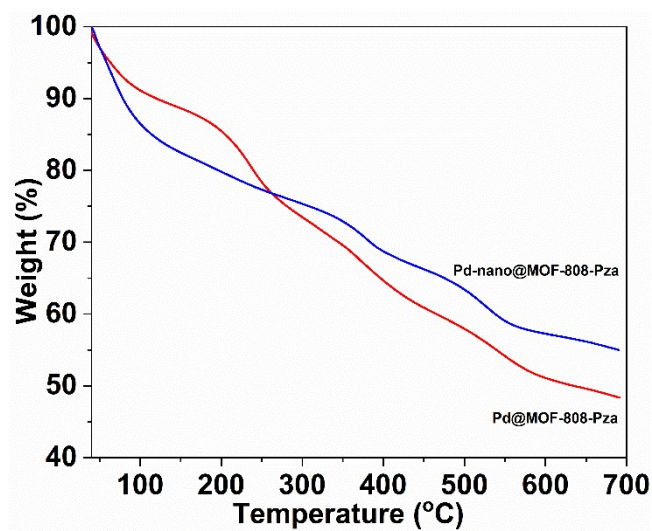**Section S1.3** Thermal gravimetric analysis (TGA).

Figure S4. TGA plots of Pd@MOF-808-Pza and Pd-nano@MOF-808-Pza, respectively.

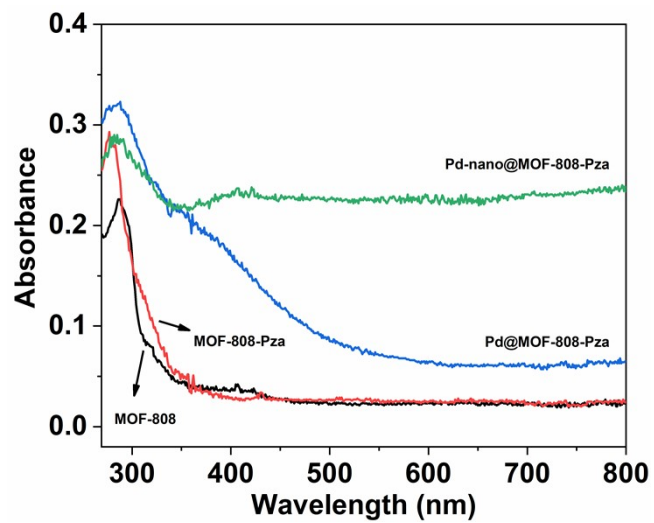**Section S1.4** UV-Vis Diffuse Reflectance Spectroscopy (UV-Vis DRS).

Figure S5. UV-Vis DRS spectra of MOF-808, MOF-808-Pza, Pd@MOF-808-Pza, and Pd-nano@MOF-808-Pza, respectively.

Section S1.5 Optical photos.

Figure S6. Graphs of bulk samples of (a) MOF-808, (b) MOF-808-Pza, (c) Pd@MOF-808-Pza, (d) Pd-nano@MOF-808-Pza, (e) Pd@MOF-808, and (f) Pd-nano@MOF-808, respectively.

Section S1.6 X-ray photoelectron spectroscopy (XPS).
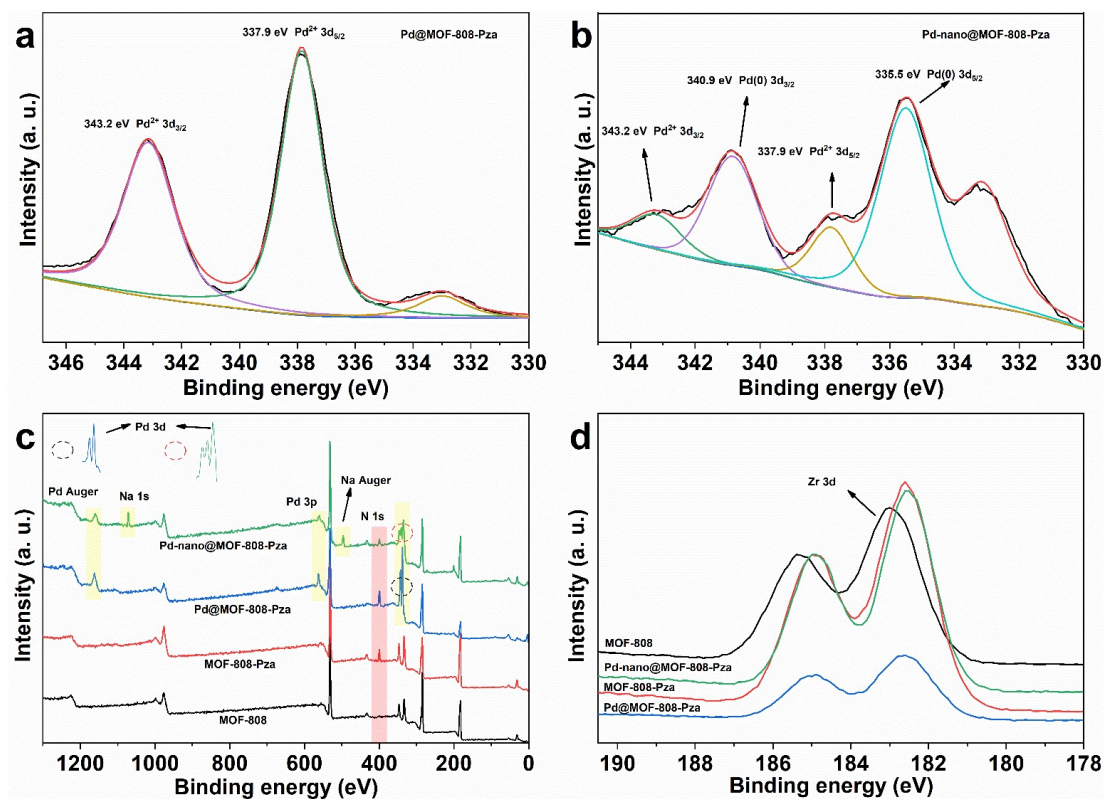
Figure S7. Pd 3d XPS spectra of Pd@MOF-808-Pza (a) and Pd-nano@MOF-808-Pza (b). Wide-scan (c) and Zr 3d (d) XPS spectra of MOF-808, MOF-808-Pza, Pd@MOF-808-Pza, and Pd-nano@MOF-808-Pza, respectively.

Section S1.7 Nuclear magnetic resonance spectroscopy (^{1}H NMR).
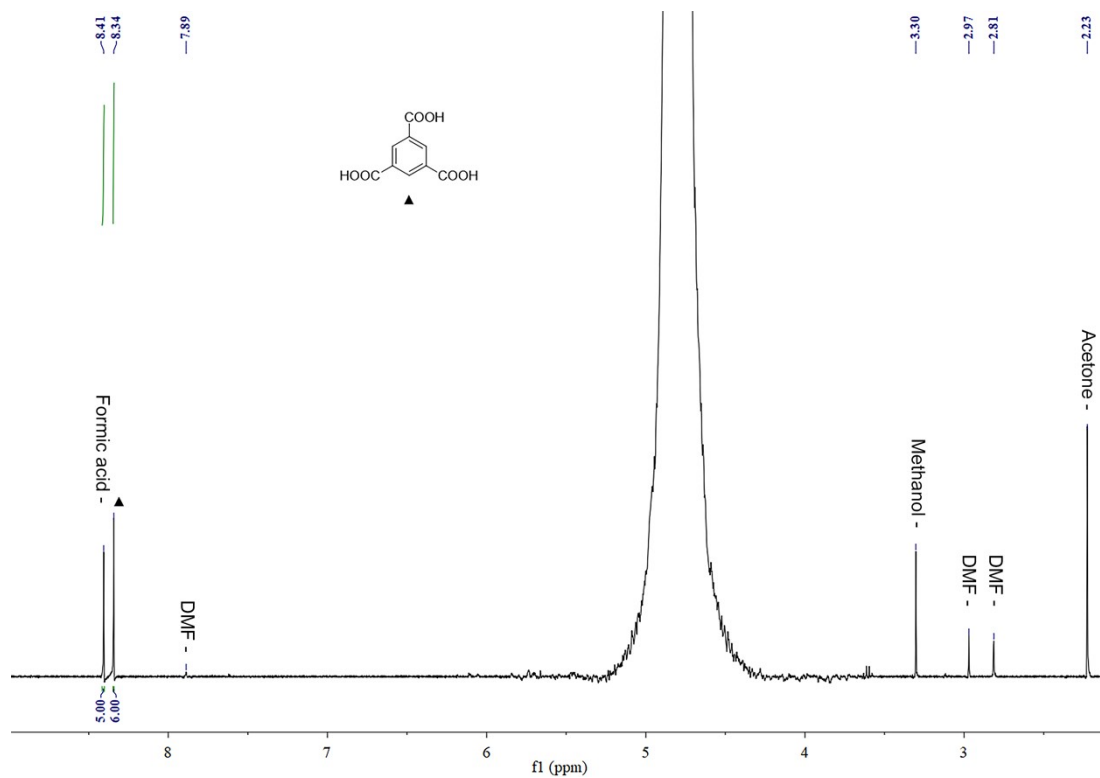
Figure S8. ^{1}H NMR spectrum of MOF-808 obtained using D_2O as solvent after alkali (NaOH) dissolution.
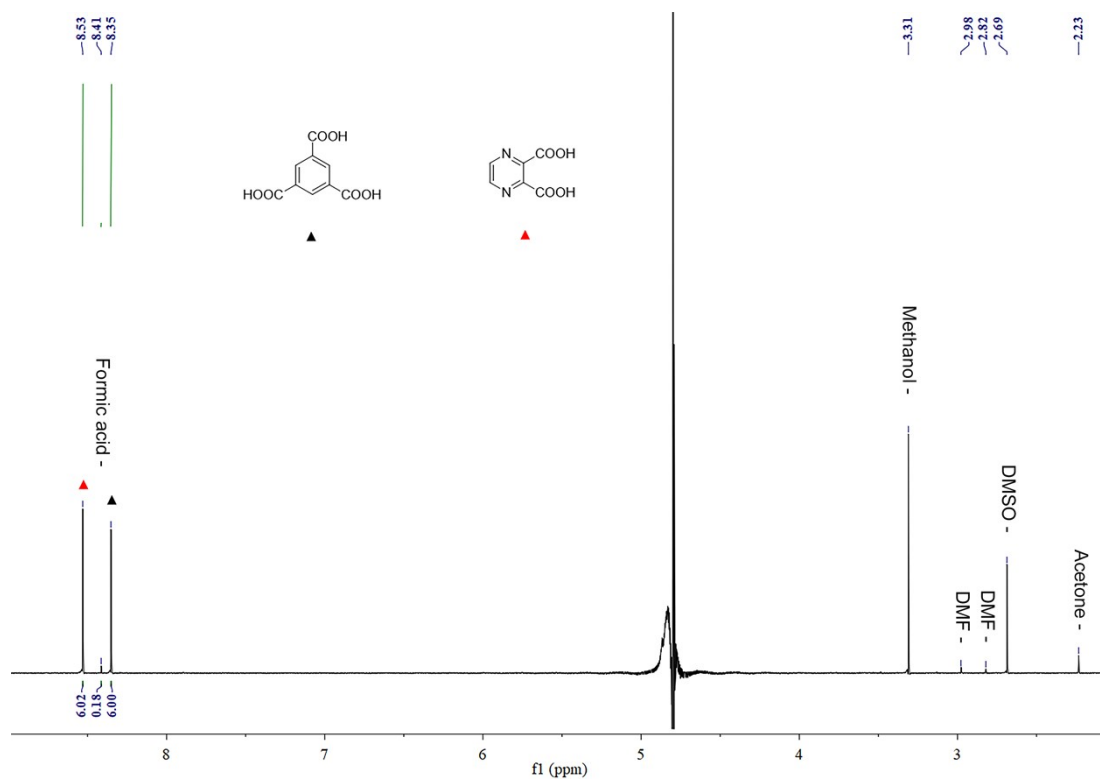
Figure S9. ^{1}H NMR spectrum of MOF-808-Pza obtained using D_2O as solvent after alkali (NaOH) dissolution.
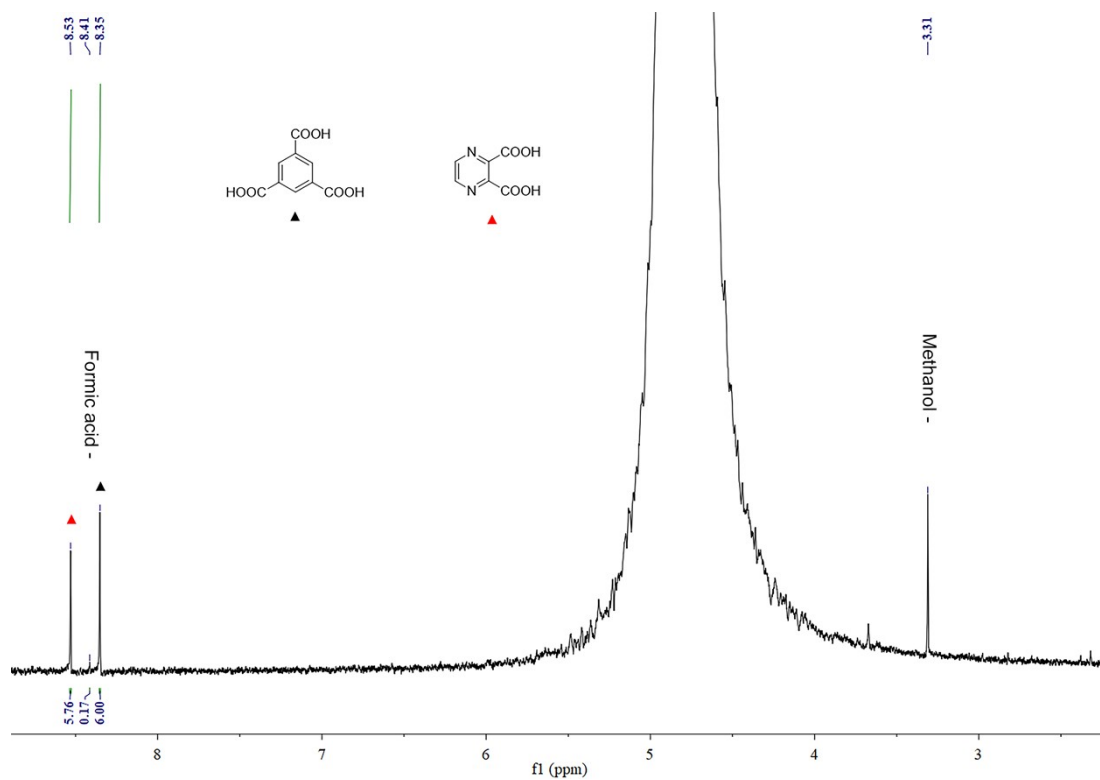
Figure S10. ^{1}H NMR spectrum of Pd@MOF-808-Pza obtained using D_2O as solvent after alkali (NaOH) dissolution.
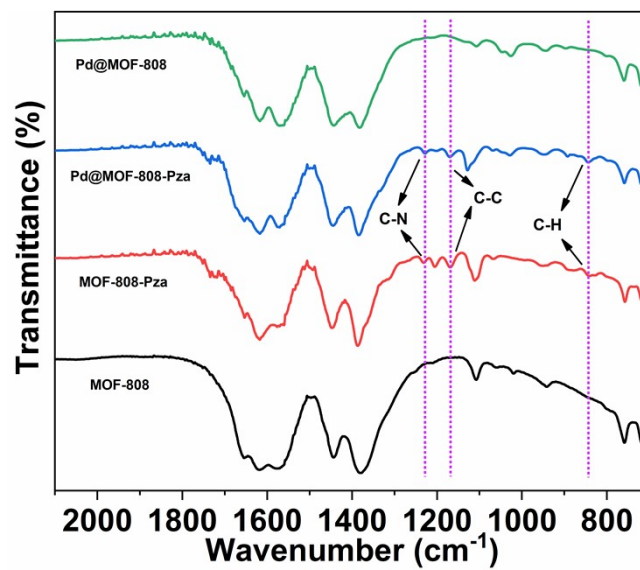
Section S1.8 FT-IR spectrum.

Figure S11. FT-IR spectra of MOF-808, MOF-808-Pza, Pd@MOF-808-Pza, and Pd@MOF-808, respectively.

Section S1.9 Energy dispersive spectroscopy (EDS).

element	Atomic percent
C	57.07
O	28.97
N	0.73
Zr	12.13
Pd	1.10
total	100

element	Atomic percent
C	52.46
O	32.22
Zr	14.97
Pd	0.35
total	100
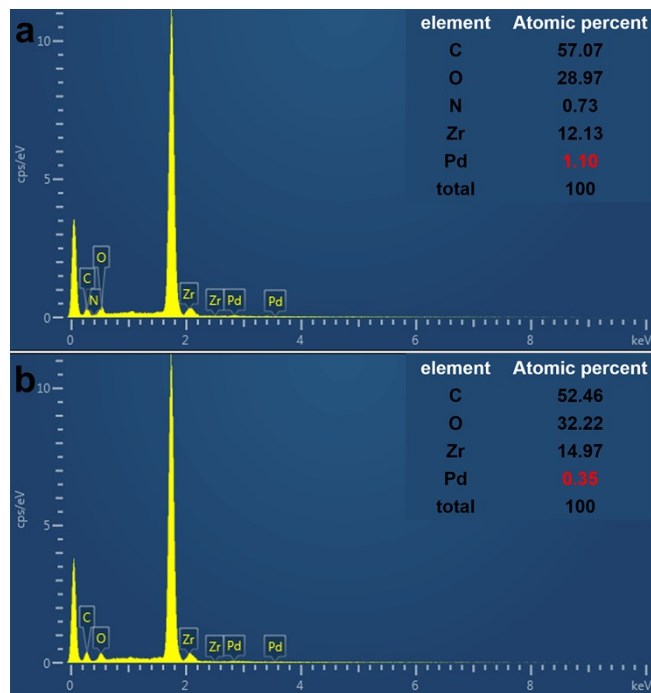
Figure S12. Element content distribution in EDS of Pd-nano@MOF-808-Pza (a) and Pd-nano@MOF-808 (b), respectively.

Section S1.10 Inductively coupled plasma mass spectrometry (ICP-MS).
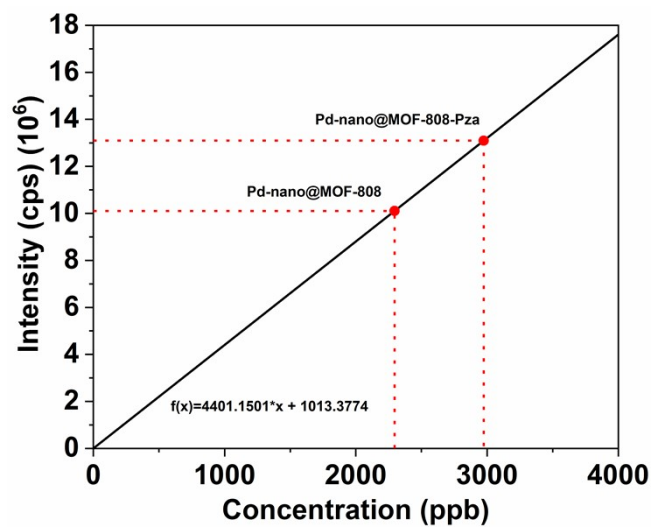
Figure S13. The content of Pd element in Pd-nano@MOF-808-Pza and Pd-nano@ MOF-808 measured by ICP-MS was determined by standard Pd^{2+} ion concentration curve.

Section S2. DFT calculations.

Table S1. Changes of total energy of Zr_6 atom clusters before and after optimization.

Model	Initial VASP energy (eV)	Relaxation energy (eV)	VASP energy (eV)
Pd@MOF-808-Pza	-467.64	-4.51	-472.15
MOF-808-Pza	-467.40	-0.31	-467.71
Pd	-	-	-1.47
Pd@MOF-808	-388.91	-1.91	-390.82
MOF-808	-	-	-386.38

Table S2. Structural parameters of Zr_6 cluster after optimization.

Model	Bond Lengths (Å)		Bond Angles (º)	
Pd@MOF-808-Pza	C(1) - C(2)	1.53	C(1) - C(2) - C(5)	128.93
	C(2) - N(1)	1.34	C(1) - C(2) - N(1)	110.17
	N(1) - C(3)	1.33	N(1) - C(3) - C(4)	122.71
	C(3) - C(4)	1.39	C(3) - C(4) - N(2)	118.78
	C(4) - N(2)	1.34	C(4) - N(2) - C(5)	119.90
	N(2) - C(5)	1.36	N(2) - C(5) - C(2)	119.51
	C(5) - C(6)	1.51	N(2) - C(5) - C(6)	115.95
	C(6) - O(1)	1.23	C(5) - C(6) - O(1)	120.80
	C(6) - O(2)	1.31	C(5) - C(6) - O(2)	115.25
	O(2) - Pd	2.06	C(6) - O(2) - Pd	114.56
	Pd - N(2)	2.04	O(2) – Pd - N(2)	81.24
			Pd - N(2) - C(5)	112.98
			Pd - N(2) - C(4)	127.11
Pd@MOF-808	C - Pd (distance)	1.91		

Table S3. Pd@MOF-808-Pza XYZ coordinates for DFT structures.
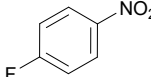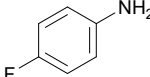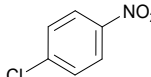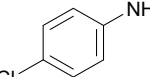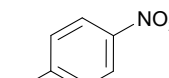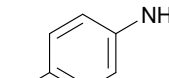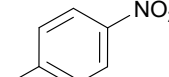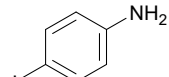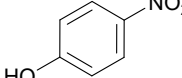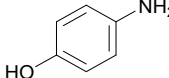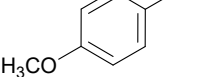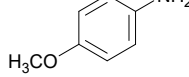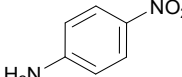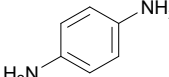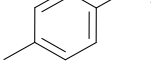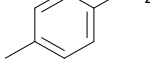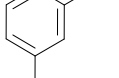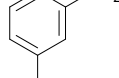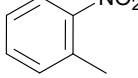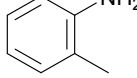
Atom	X	Y	Z	Atom	X	Y	Z
N1	0.7569	0.6769	0.5325	C11	0.4599	0.3426	0.5171
N2	0.6445	0.6365	0.4561	C12	0.2382	0.6216	0.4583
C1	0.7441	0.6915	0.4508	C14	0.3278	0.7066	0.6782
C2	0.6879	0.6690	0.4129	C17	0.4347	0.6876	0.4412
C3	0.7145	0.6425	0.5776	O27	0.3769	0.5850	0.7253
C4	0.6565	0.6241	0.5389	O28	0.2937	0.5060	0.5212
H1	0.7780	0.7205	0.4161	O29	0.4762	0.5673	0.5052
H2	0.6777	0.6778	0.3456	O30	0.3114	0.4819	0.6900
C5	0.7344	0.6266	0.6680	O31	0.4939	0.5432	0.6741
O1	0.7905	0.6483	0.6924	O34	0.4107	0.4642	0.4699
O2	0.6995	0.5953	0.7137	O35	0.4641	0.5593	0.8371
Zr1	0.4126	0.4951	0.7485	O38	0.2331	0.4177	0.5920
Zr4	0.3404	0.4265	0.5711	O40	0.5310	0.4824	0.4195
Zr6	0.4990	0.4797	0.5573	O41	0.1990	0.5121	0.6343
Zr7	0.2887	0.5695	0.6380	O43	0.4856	0.6437	0.7558
Zr9	0.4473	0.6227	0.6242	O46	0.4502	0.5324	0.3471
Zr12	0.3750	0.5541	0.4468	O53	0.3236	0.4899	0.3581
O3	0.5034	0.4476	0.7814	O54	0.5544	0.6315	0.6032
O6	0.3320	0.3615	0.6783	O55	0.2566	0.5669	0.7758
O8	0.5019	0.3836	0.5187	O56	0.5887	0.5371	0.5611
O9	0.2288	0.6115	0.5368	O57	0.3020	0.4055	0.4395
O11	0.3876	0.6998	0.6676	O58	0.3375	0.5168	0.8482
O14	0.4092	0.6436	0.4030	C24	0.4867	0.6129	0.8258
O21	0.2843	0.6017	0.4139	C27	0.1898	0.4561	0.6154
O22	0.4556	0.6877	0.5170	C29	0.5049	0.5048	0.3516
O23	0.2857	0.6656	0.6765	C33	0.3008	0.4363	0.3694
O24	0.5588	0.4377	0.6585	C34	0.5978	0.5931	0.5798
O25	0.4000	0.3494	0.5277	C35	0.2828	0.5444	0.8437
O26	0.3784	0.4056	0.7923	O59	0.4330	0.4287	0.6443
C6	0.5494	0.4277	0.7369	O61	0.3546	0.6205	0.5509
C9	0.3529	0.3617	0.7541	Pd1	0.8370	0.6995	0.6013

Table S4. Pd@MOF-808 XYZ coordinates for DFT structures.

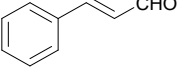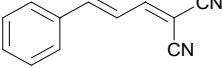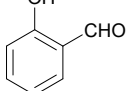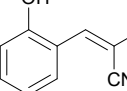| Atom	X	Y	Z	Atom	X	Y	Z
Zr1	0.4126	0.4951	0.7485	O29	0.4762	0.5673	0.5052
Zr4	0.3404	0.4265	0.5711	O30	0.3114	0.4819	0.6900
Zr6	0.4990	0.4797	0.5573	O31	0.4939	0.5432	0.6741
Zr7	0.2887	0.5695	0.6380	O34	0.4107	0.4642	0.4699
Zr9	0.4473	0.6227	0.6242	O35	0.4641	0.5593	0.8371
Zr12	0.3750	0.5541	0.4468	O38	0.2331	0.4177	0.5920
O3	0.5034	0.4476	0.7814	O40	0.5310	0.4824	0.4195
O6	0.3320	0.3615	0.6783	O41	0.1990	0.5121	0.6343
O8	0.5019	0.3836	0.5187	O43	0.4856	0.6437	0.7558
O9	0.2288	0.6115	0.5368	O46	0.4502	0.5324	0.3471
O11	0.3876	0.6998	0.6676	O53	0.3236	0.4899	0.3581
O14	0.4092	0.6436	0.4030	O54	0.5544	0.6315	0.6032
O21	0.2843	0.6017	0.4139	O55	0.2566	0.5669	0.7758
O22	0.4556	0.6877	0.5170	O56	0.5887	0.5371	0.5611
O23	0.2857	0.6656	0.6765	O57	0.3020	0.4055	0.4395
O24	0.5588	0.4377	0.6585	O58	0.3375	0.5168	0.8482
O25	0.4000	0.3494	0.5277	C24	0.4867	0.6129	0.8258
O26	0.3784	0.4056	0.7923	C27	0.1898	0.4561	0.6154
C6	0.5494	0.4277	0.7369	C29	0.5049	0.5048	0.3516
C9	0.3529	0.3617	0.7541	C33	0.3008	0.4363	0.3694
C11	0.4599	0.3426	0.5171	C34	0.5978	0.5931	0.5798
C12	0.2382	0.6216	0.4583	C35	0.2828	0.5444	0.8437
C14	0.3278	0.7066	0.6782	O59	0.4330	0.4287	0.6443
C17	0.4347	0.6876	0.4412	O61	0.3546	0.6205	0.5509
O27	0.3769	0.5850	0.7253	Pd1	0.5260	0.6508	0.9223
O28	0.2937	0.5060	0.5212				
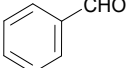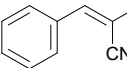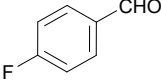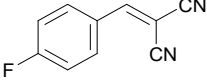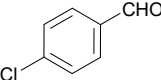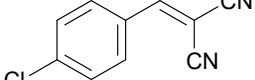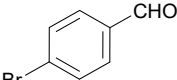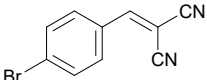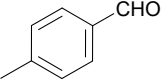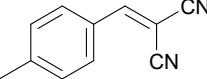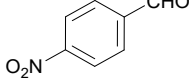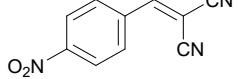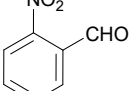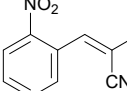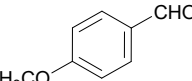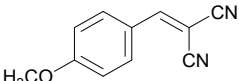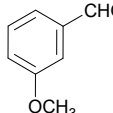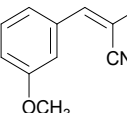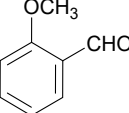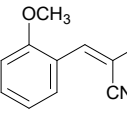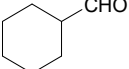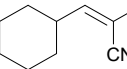
Section S3. Catalytic performance.

Table S5. The reduction activity of Pd@MOF-808-Pza for nitrobenzene derivatives. [a]

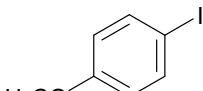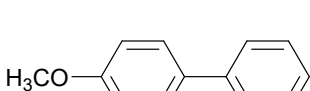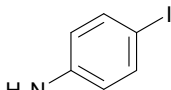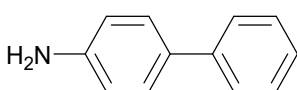| Entry	Reactant	Product	Yield (%)	TOF (h^{-1})
1	(nitrobenzene)	(aniline)	> 99	215.83
2	(4-fluoronitrobenzene)	(4-fluoroaniline)	92.54	199.73
3	(4-chloronitrobenzene)	(4-chloroaniline)	59.95	129.39
4	(4-bromonitrobenzene)	(4-bromoaniline)	0	0
5	(4-iodonitrobenzene)	(4-iodoaniline)	0	0
6	(4-nitrophenol)	(4-aminophenol)	> 99	215.83
7	(4-nitroanisole)	(4-methoxyaniline)	> 99	215.83
8	(4-nitroaniline)	(1,4-phenylenediamine)	> 99	215.83
9	(4-nitrotoluene)	(4-methylaniline)	> 99	215.83
10	(3-nitrotoluene)	(3-methylaniline)	86.75	187.23
11	(2-nitrotoluene)	(2-methylaniline)	89.53	193.23
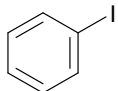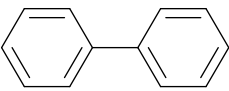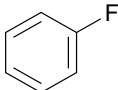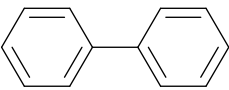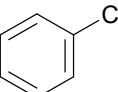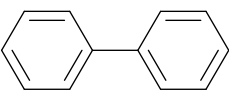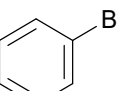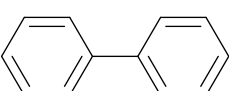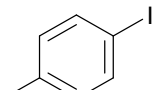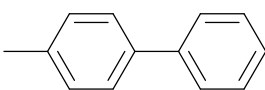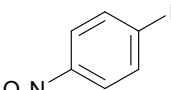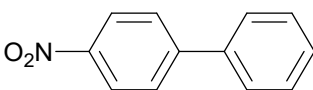
[a] Reaction conditions: 0.5 mmol reactant, 0.75 mmol NaBH$_4$, 25 °C, 10 min, 10 mg Pd@MOF-808-Pza catalyst, 15 mL of ethanol.

Table S6. The catalytic activity of Pd@MOF-808-Pza for Knoevenagel condensation. [a]

Entry	Reactant	Product	Yield (%)	TOF (h⁻¹)
1			94.35	67.88
2			51.37	36.96
3			86.96	62.56
4			93.90	67.55
5			52.59	37.83
6			86.46 [b]	62.20
7			82.23	59.16
8			30.54	21.97
9			58.94	42.40
10			72.28	52.00
11			64.90	46.69
12			62.72	45.12
13			78.44	56.43
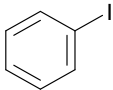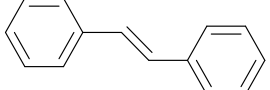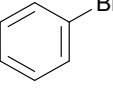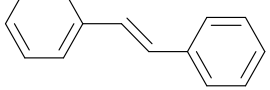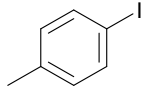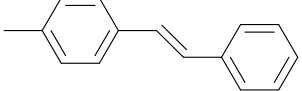
[a] Reaction conditions: 0.5 mmol reactant, 0.6 mmol malononitrile, 25 °C, 30 min, 10 mg Pd@MOF-808-Pza catalyst, 15 mL of ethanol. [b] The other 13.54% are amino products.

Table S7. The catalytic activity of Pd@MOF-808-Pza for Suzuki reaction. [a]

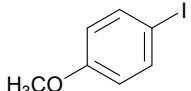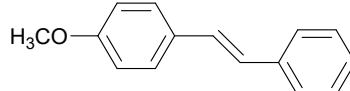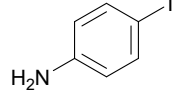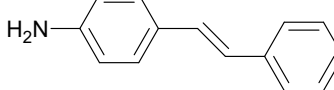

Entry	Reactant	Product	Yield (%)	TOF (h^{-1})
1			> 99	8.99
2			20.96	1.88
3			32.15	2.89
4			> 99	8.99
5			> 99	8.99
6			92.52	8.32
7			> 99	8.99
8			78.37	7.05

[a] Reaction conditions: 0.5 mmol reactant, 0.6 mmol phenylboronic acid, 80 °C, 10 mg Pd@MOF-808-Pza catalyst, 15 mL of DMF, anhydrous.

Table S8. The catalytic activity of Pd@MOF-808-Pza for Heck reaction. [a]

Entry	Reactant	Product	Yield (%) [b]
1			92.57
2			33.41
3			96.27
4			>99
5			75.12

[a] Reaction conditions: 0.5 mmol reactant, 0.6 mmol styrene, 80 °C, 10 mg Pd@MOF-808-Pza catalyst, 15 mL of DMF, anhydrous; [b] Catalytic reaction products were analyzed and identified by GC-MS.